Time-Reversal Imaging for Wideband Underwater Target Classification

Hongwei Liu, Nilanjan Dasgupta and *Lawrence Carin*

Department of Electrical and Computer Engineering,
Duke University, Durham, NC 27708-0291

ABSTRACT

Time-reversal imaging is addressed for sensing an elastic target situated in an acoustic waveguide. It is demonstrated that the channel parameters associated with a given measurement may be determined via a genetic-algorithm (GA) search in parameter space. Target classification based on time-reversal imagery is considered, with this implemented via a relevance-vector machine.

1. INTRODUCTION

The use of acoustic backscattered signals to detect and classify underwater targets has attracted significant attention in recent years [1-7]. This involves discrimination between targets and non-targets as well as from background clutter (e.g. surface roughness). There are several factors that make the underwater detection and classification processes a challenging problem. First, the target scattered signal is distorted by multi-path propagation, which is dependent on the environmental acoustic parameters, such as target and receiver location, water depth, and seabed geoacoustic parameters. Consequently, an efficient algorithm is needed to recover the target scattered signatures or extract features which are independent of such channel parameters. Second, the target scattered signal may be submerged by the competing clutter caused by biological sources in the water column, surface and bottom reverberation effects and system noise. A signal processing algorithm is required to enhance the target scattered signal from background noise and clutter. Generally, we only have prior knowledge about the target to be detected or classified, and lack prior knowledge of the false targets.

Recently, the Time-reversal mirror (TRM) [8] has been demonstrated in underwater acoustic environments [9,10], with this also referred to as phase conjugation in the frequency domain. TRM has significant potential for underwater communications. The same principal may be exploited in the context of imaging. In this paper we consider time-reversal imaging of elastic targets situated in an acoustic waveguide. A relevance vector machine (RVM) [11] classifier is built to identify mine-like targets from false targets in a shallow water channel, based on the TRM imagery. The paper is organized as follows: In section 2, we discuss time-reversal theory for an extended target. In section 3, a channel inversion algorithm based on a GA and TRM imagery is developed. In section 4, we present the in-channel classification problem in detail including RVM classifier design and feature extraction. Example results are presented in section 5, followed in section 6 by conclusions.

2. TIME-REVERSAL THEORY

The displacement potential ψ is related to the displacement $\boldsymbol{u}$ via $\boldsymbol{u}=\nabla\psi$. Assume that a target is defined by a surface *S*, and this surface resides within a medium characterized by Green's function $G(\boldsymbol{r},\boldsymbol{r}')$, for observation point $\boldsymbol{r}$ and source point $\boldsymbol{r}'$. Assuming that the normal component of displacement on the target surface is negligible (rigid target), we have

$$\psi(\boldsymbol{r}) = -\int_S \psi(\boldsymbol{r}')\frac{\partial G(\boldsymbol{r},\boldsymbol{r}')}{\partial n'}dS' + \psi_{\text{inc}}(\boldsymbol{r};\boldsymbol{r}_s) \quad (1)$$

where $\psi_{\text{inc}}(\boldsymbol{r};\boldsymbol{r}_s)$ represents the incident fields. We simplify the discussion by first considering an infinite homogenous medium characterized by wavenumber *k*, and therefore $(\nabla^2+k^2)G(\boldsymbol{r},\boldsymbol{r}')=-\delta(\boldsymbol{r}-\boldsymbol{r}')$. For this case (1) becomes

$$\psi(\boldsymbol{r}) = -\int_S u(\boldsymbol{r},\boldsymbol{r}',\boldsymbol{r}_s)\psi_{\text{inc}}(\boldsymbol{r}';\boldsymbol{r}_s)G(\boldsymbol{r},\boldsymbol{r}')dS' + \psi_{\text{inc}}(\boldsymbol{r};\boldsymbol{r}_s) \quad (2)$$

where

$$u(\boldsymbol{r},\boldsymbol{r}',\boldsymbol{r}_s) \equiv -\psi(\boldsymbol{r}')\frac{\partial G(\boldsymbol{r},\boldsymbol{r}')}{\partial n'} / \left[\psi_{\text{inc}}(\boldsymbol{r}';\boldsymbol{r}_s)\left(jk+1/|\boldsymbol{r}-\boldsymbol{r}'|\right)\right] \quad (3)$$

By including $\psi_{\text{inc}}(\boldsymbol{r}';\boldsymbol{r}_s)$ explicitly within the integral in (2), we directly account for the fast phase variation of $\psi(\boldsymbol{r}')$ due to the excitation field. The term $u(\boldsymbol{r},\boldsymbol{r}';\boldsymbol{r}_s)$ has relatively slow-varying phase.

Using $\psi_{\text{inc}}(\boldsymbol{r}';\boldsymbol{r}_s) = -G(\boldsymbol{r}',\boldsymbol{r}_s)$, and assuming that the incident field is zero (or may be eliminated) at the receiver position $\boldsymbol{r}$, then (2) may be expressed as

$$\psi(\boldsymbol{r};\boldsymbol{r}_s) = \int_S u(\boldsymbol{r},\boldsymbol{r}',\boldsymbol{r}_s)G(\boldsymbol{r}',\boldsymbol{r}_s)G(\boldsymbol{r},\boldsymbol{r}')dS' \quad (4)$$

where in (4) we note explicitly the dependence of the scattered fields on both the source and receiver positions, $\boldsymbol{r}_s$ and $\boldsymbol{r}$, respectively.

In the following discussion we assume that the target is large enough with respect to wavelength such that a

stationary-phase analysis of the integral in (4) is appropriate. Assuming M stationary points, for the kth receiver of a linear array in water channel, we have

$$\psi(\boldsymbol{r}_k;\boldsymbol{r}_s) \approx \sum_{m=1}^{M} \hat{u}_m(\boldsymbol{r}_k,\boldsymbol{r}'_m,\boldsymbol{r}_s) G(\boldsymbol{r}'_m,\boldsymbol{r}_s) G(\boldsymbol{r}'_m,\boldsymbol{r}_k) \quad (5)$$

where $\hat{u}(\boldsymbol{r},\boldsymbol{r}'_m,\boldsymbol{r}_s)$ accounts for the new factors associated with the stationary-phase analysis.

Using multiple receivers, our goal is to image the M scattering centers. We perform this via phase conjugation of (5), in the frequency domain, and then this signal is propagated numerically into the computational domain, from the receiver at $\boldsymbol{r}_k$. This process accounts for propagation from the scattering centers to the receiver. To account for propagation from the source to the scattering center, we also multiply the aforementioned phase-conjugated response by the response of propagation from the source to the scattering center.

Performing the above phase conjugation, accounting for propagation from the source $\boldsymbol{r}_s$ and the receiver $\boldsymbol{r}_k$ to point $\boldsymbol{r}$ in the image domain, and finally performing an inverse Fourier transform to convert the signal to the time domain, we obtain the space-time signal

$$I_s(\boldsymbol{r},t) = \sum_{k=1}^{K} \psi^*(\boldsymbol{r}_k;\boldsymbol{r}_s) G_{TR}(\boldsymbol{r},\boldsymbol{r}_s) G_{TR}(\boldsymbol{r}_k,\boldsymbol{r}) \exp(j\omega t) d\omega \quad (6)$$

It is important that the channel parameters associated with G_{TR} are consistent with the actual channel parameters

The time-reversal image $I_s(\boldsymbol{r},t)$ is a four-dimensional quantity (space-time). In this paper, we only use space-dependent image for classification and channel inversion, which is defined as

$$\hat{\mathrm{I}}_s(i,j) \equiv \mathrm{I}_s(i,j,t=0) \quad (7)$$

where (i,j) denoted the sampled points in two-dimensional space (down range and water depth).

3. CHANNEL INVERSION ALGORITHM

We employ the time-reversal image itself to estimate the appropriate parameters for G_{TR}. Assume channel parameters Φ are employed in G_{TR}, and that the associated time-reversal image is represented as $\hat{\mathrm{I}}_s(i,j,\Phi)$. We treat the inversion for the channel parameters as an optimization problem, and find the set of parameters from the defined search space, which minimize a cost function defined in terms of $\hat{\mathbf{I}}_s(i,j,\Phi)$. Genetic algorithms (GA) and simulated annealing (SA) are two general techniques for multi-dimensional optimization problems, and these have been used for acoustic-channel inversion [12,13].

Define the equivalent probability mass function

$$p(i,j;\Phi) = \frac{\left|\hat{\mathbf{I}}_s(i,j;\Phi)\right|}{\sum_{(i,j)\in\Lambda} \left|\hat{\mathbf{I}}_s(i,j;\Phi)\right|} \quad (8)$$

If the image is tightly focused about the strong scatterer located in the region Λ, the $\mathrm{p}(i,j;\Phi)$ should have low entropy. By contrast, the entropy increases as the image defocuses. The first component of the GA cost function is the entropy of $\mathrm{p}(i,j;\Phi)$, defined as

$$\mathrm{E}_1(\Phi) = -\sum_{(i,j)\in\Lambda} \mathrm{p}(i,j;\Phi) ln \mathrm{p}(i,j;\Phi) \quad (9)$$

The second component of the cost function is analogous to that discussed in [12,13]. Let $r_k(\omega_n)$ represent the scattered signal measured at receiver k, for frequency ω_n. Further, let $c_k(\omega_n;i,j,\Phi)$ represent the *computed* scattered response at frequency ω_n, for a point scatterer located at a point $(i,j)\in\Lambda$. Assuming N_f frequencies, the second component to the cost function is

$$E_2(\Phi) = 1 - \max_{(i,j)\in\Lambda} \left(\frac{1}{N_f} \sum_{n=1}^{N_f} \frac{\left|\sum_{k=1}^{K} r_k(\omega_n) c_k(\omega_n;i,j,\Phi)\right|^2}{\sum_{k=1}^{K} |r_k(\omega_n)|^2 \sum_{k=1}^{K} |c_k(\omega_n;i,j,\Phi)|^2} \right) \quad (10)$$

and the total cost function is $\mathrm{E}(\Phi) = \mathrm{E}_1(\Phi) + \gamma \mathrm{E}_2(\Phi)$. A genetic algorithm (GA) is employed to determine those parameters Φ that minimize $\mathrm{E}(\Phi)$, and we have found that setting $\gamma = 1$ yields good results.

4. TARGET CLASSIFICATION

We now consider target classification based on TRM image data. Five distinct objects are considered in the channel. Two of the targets are deemed "targets of interest", and the other three are deemed "false targets". The targets of interest are defined as hypothesis one (H_1), and the false targets are the null hypothesis, H_o.

4.1 Feature extraction

The classification is performed on the signal $\hat{I}_s(i,j;\Phi)$. Specifically, we fix the depth j and view the data as a function of range i, for simplicity. In the examples presented below we assume the target depth j is known, for simplicity, although this can be estimated from the data.

When we process the time-reversal signature $\hat{I}_s(i,j;\Phi)$, for fixed j and variable i, we have range-dependent data. The features are extracted from this data. In particular, assume that $d(i)$ represents the range-dependent data, where i denotes the range index. The first type of features are based on moments of $d(i)$. In particular, the positional probability density function $p(i)$ and central moments m_l are calculated as

$$p(i) = \frac{d^2(i)}{\sum_{i=1}^{I} d^2(i)} \quad , \quad m_1 = \sum_{i=1}^{I} i p(i) \quad , \quad m_{k>1} = \sum_{i=1}^{I} (i-m_1)^k p(i) \quad (11)$$

where we assume I range samples of interest. We do not use the first moment m_1 (or mean) as a feature, since it changes with a change in the target-sensor distance.

In addition, we consider features based on the spectral (Fourier) properties of $d(i)$. In this case the Fourier transform of $d(i)$ is uniformly divided into a set of

frequency bands, and the features are the energy within each band.

4.2 Relevance vector machine (RVM) classifier

Given a feature vector $\boldsymbol{v}$, our goal is to perform classification based on the probability that $\boldsymbol{v}$ is associated with hypotheses H_o and H_1, denoted respectively $p(H_o|\boldsymbol{v})$ and $p(H_1|\boldsymbol{v})$. Since the false targets constitute an infinite set, we here assume no knowledge of $p(H_o|\boldsymbol{v})$. Hence the classification is performed based entirely on $p(H_1|\boldsymbol{v})$, representative of the targets we expect to encounter. In addition, we design a single classifier for the two targets.

Assume that we have access to "training" data $\{\boldsymbol{v}_n\}_{n=1,N}$, representative of example feature vectors from the target(s) of interest, all characteristic of hypothesis H_1. We define the function

$$f(\boldsymbol{v};\boldsymbol{w}) = \sum_{n=1}^{N} w_n g(\boldsymbol{v},\boldsymbol{v}_n) + w_o \tag{12}$$

where $g(\boldsymbol{v},\boldsymbol{v}_n)$ is a kernel that quantifies the similarity between feature vectors $\boldsymbol{v}$ and $\boldsymbol{v}_n$. The w_n are weights, cumulatively represented by the vector $\boldsymbol{w}$, which define the importance of training feature vector $\boldsymbol{v}_n$ on the classifier, defined in terms of $f(\boldsymbol{v};\boldsymbol{w})$. The probability that feature vector $\boldsymbol{v}$ is associated with H_1, for given weights $\boldsymbol{w}$, is defined in terms of the logistic link function

$$p(H_1|\boldsymbol{v},\boldsymbol{w}) \equiv \frac{\exp[f(\boldsymbol{v};\boldsymbol{w})]}{1+\exp[f(\boldsymbol{v};\boldsymbol{w})]} \tag{13}$$

The relevance-vector machine (RVM) [11] is a design procedure to optimize weights $\boldsymbol{w}$ and the "most-relevant" training examples $\boldsymbol{v}_n$ (those with non-zero weights). The RVM has proven to be an effective tool because it seeks to achieve two competing objectives: (i) maximization of (14) for feature vectors $\boldsymbol{v}$ in the training set $\{\boldsymbol{v}_n\}_{n=1,N}$, while (ii) the sparseness prior forces most of the weights w_n in (12) to vanish. The details of the RVM may be found in [11].

5. EXAMPLE RESULTS

5.1 Example results with measured data

The data was collected in a bay near Panama City, FL, USA, and the channel depth was approximately 8 m, and the range between the sensors and targets was approximately 20 m. The system consisted of a vertical array of 12 receivers, with an isotropic source situated at the midpoint of the array. The middle of the array was 3.4 m below the air-water interface, and the sensor bandwidth was 1.3-10 KHz. The receivers platform moves along a straight line and records a sequence of observations for different target-receiver orientations. Based on the measured acoustical response, we estimate the channel parameters, employing a GA and the cost function discussed above. Then, we synthesize the TRM images based on estimated channel parameters.

The channel parameters Φ considered were the water depth, water sound speed, sound speed in the bottom, the density of the bottom, and the attenuation of the bottom. In Table 1 we present a comparison between the parameters Φ extracted via the GA, and estimates of channel parameters based on estimations made at the experiment site. We see from Table 1 that the water depth, the water sound speed, and bottom sound speed are in good agreement with on-site estimations. In Fig. 2(b) we present the TRM imaging result of in-channel data, based on estimated channel parameters in Table 1, comparing with raw data (before TRM processing) in Fig. 2(a). The TRM image is synthesized in cross-range (corresponds to the position of the receiver array) and down-range (corresponds to the target-receiver distance which is parallel to the bottom) domain, for a given target depth, which is estimated using GA. We see that the targets scattered signals are well focused after TRM imaging, and the signal noise ratio is improved significantly as well.

5.2 Classification results with synthesized data

The measurement did not consider a sufficient number of targets and false targets for statistically meaningful classification results, and therefore the subsequent results are based on synthesized data. The wideband bistatic scattered fields are computed for all targets via a free-field finite-element method (FEM) simulation. The channel response is calculated using a modal channel model. The target-receiver distance (parallel to the bottom) ranges from 50 to 200 meters. A 28-element linear array receiver is employed perpendicular to the bottom. The array is 2 meters long and its center is situated 4 meters above the sea bottom. The center of each target is located 0.18 m above the sea bottom. A two-layer geoacoustic model is considered (see Fig. 1). The data covers the frequency band 50 Hz to 10 KHz. Each of the five targets is rotated about its axis over 360^o, with 1^o angular sampling, thereby constituting multiple synthesized measurements. The RVM classifier is trained using data of distance 100 m, and tested for distance of 50, 75, 125, 150 and 200 m. It is assumed in all cases that the channel parameters are known exactly when performing time-reversal imaging. The classification results are shown in Fig. 3(a). The multiple observations are fused using the linear method (sum over the SVM outputs for multiple observations), and angular sampling is 5 degree. Fig. 3(b) shows the classification results for the cases that channel parameters are not known exactly, the TRM imaging is performed based on the GA estimated channel parameters, 10 independent GA runs are considered in Fig. 3(b).

6. CONCLUSIONS

Time-reversal imaging was addressed for sensing an elastic target situated in an acoustic waveguide. The theory of wideband time-reversal imaging of an extended target is investigated. It is demonstrated that the channel parameters associated with a given measurement may be determined via a genetic-algorithm (GA) search in parameter space, employing a cost function based on the time-reversal image quality. Example GA channel-parameter-inversion results are presented for measured data. Target classification based on time-reversal imagery is also considered for the synthesized data. The classifier is implemented via a relevance-vector machine.

REFERENCES

[1] R.P. Gorman, T. J. Sejnowski, "Learned classification of sonar targets using a massively parallel network", IEEE Trans. Acoust., Speech, Signal Processing, Vol. 36, No. 7, July 1988

[2] M.R. Azimi-Sadjadi, Q. Huang, and G. Dobeck, "Underwater target classification using multiaspect fusion and neural network", Proc. SPIE Int. Symp. Aerospace/Defense Sensing Contr, Orlando, FL, Apr. 1998, pp.334-341

[3] M.R. Azimi-Sadjadi, D. Yao, Q. Huang, and G. Dobeck, "Underwater target classification using wavelet packets and neural networks", IEEE Trans. Neural Networks, Vol.11, No.3, May 2000, pp:784-794

[4]H. W. Liu and L. Carin, "Class-based target classification in shallow water channel based on Hidden Markov Model", Proc. IEEE International conference on acoustics, speech and signal processing , May 2002, Orlando, FL, pp.2889-2892

[5]P.R. Runkle, P. K. Bharadwaj, L. Couchman and L. Carin, "Hidden Markov Models for multi-aspect targets classification", IEEE Trans. Signal Processing,Vol.47, July,1999, pp.2035-2040

[6]P. K. Bharadwj, P. R. Runkle and L. Carin, "Target identification with wave-based matched pursuits and Hidden Markov Models", IEEE Trans. Antenna and Propagation, Vol. 47, Oct. 1999, pp.1543-1554

[7]N. Dasgipta, P.K.Bharadwaj, L. Couchman and L. Carin, "Dual Hidden Markov Model for characterizing wavelet coefficients from multi-aspect scattering data", Signal Processing, Vol. 81, 2001, pp. 1303-1316

[8]M. Fink, "Time-reversal acoustics", Physics Today, Vol.50, 1997, pp.34-40

[9]W. A. Kuperman, W. S. Hodgkiss, H. C. Song, T. Akal, C. Ferla, and D. R. Jackson, "Phase conjugation in the ocean: Experimental demonstration of an acoustic time reversal mirror", J. Acoust. Soc. Am, Vol.103, 1998, pp. 25-40

[10]J. S. Kim, H. C. Song, and W. A. Kuperman, "Adaptive time-reversal mirror", J. Acoust. Soc. Am, Vol.109, 2001, pp.1817-1825

[11]M.E.Tipping, "Sparse Bayesian learning and the relevance vector machine", Journal of Machine Learning Research, No. 1, 2001, pp.211-214

[12]P. Gerstoft, "Ocean acoustic inversion with estimation of a posteriori probability distributions", J. Acoust. Soc. Am., Vol.104, Aug. 1998, pp.808-819

[13]S. E. Dosso, M. L. Yeremy, J. M. Ozard, and N. R. Chapman, "Estimation of ocean bottom properties by matched-field inversion of acoustic field data", IEEE Journal of Ocean Engineering, Vol.18, July 1993, pp.232-239

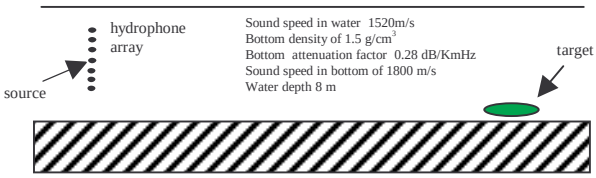

Fig. 1 Channel model

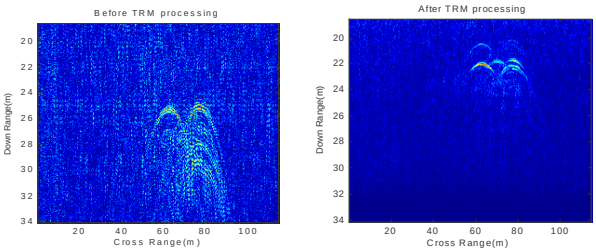

(a) (b)

Fig. 2 Measured in-channel data (a)before TRM processing (b) after TRM processing for a given target depth, using the channel parameters estimated in Table. 1

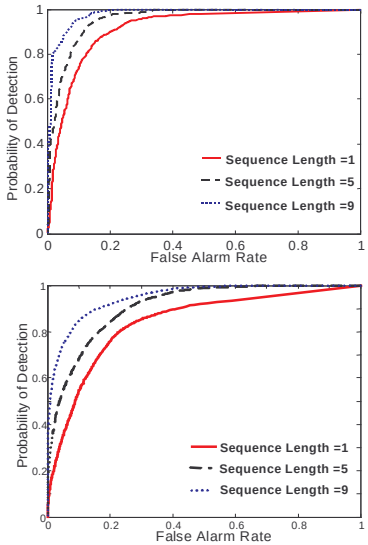

(a)

(b)

Fig. 3 Classification results based on TRM images, classifier is trained using data of distance 100 m, and tested for distance of 50, 75, 125, 150 and 200 m. (a) TRM imaging performed with known channel parameters (b) TRM imaging performed with GA estimated channel parameters

Table 1. Channel inversion results

	Prior value	Estimated	Search range
Water depth(m)	8.23	8.3	(7.73,8.73)
Sound Speed in water(m/s)	1490	1489.21	(1440,1540)
Sound Speed in bottom(m/s)	1705	1655.25	(1605 ,1805)
Density of bottom(g/cm^3)	N/A	3.086	(1,3.5)
Attenuation of bottom(dB/kmHz)	N/A	0.504	(0.1 ,0.9)